A 3D MONTE-CARLO (POTTS) MODEL FOR RECRYSTALLIZATION AND GRAIN GROWTH IN POLYCRYSTALLINE MATERIALS

O.M. IVASISHIN, N.L. VASILIEV, S.V. SHEVCHENKO, S.L. SEMIATIN[1]

UDC 004.94:519.245:548.53

Institute for Metal Physics, Nat. Acad. Sci. of Ukraine
(36, Academician Vernadsky Str., Kyiv 03142, Ukraine; e-mail: shevchsv@imp.kiev.ua),
[1]**Air Force Research Laboratory, AFRL/MLLM**
(Wright-Patterson Air Force Base, OH 45433-7817, USA)

The recrystallization of polycrystalline metallic materials is modeled by using a 3D Monte-Carlo (Potts) approach, in which the initial microstructure, texture [orientation-distribution function (ODF)], spatial distribution of the stored energy of deformation, and nucleation mechanism are carefully quantified. The formation of a microstructural and textural inhomogeneity due to the recrystallization in deformed single-phase metallic materials is thus predicted. The modeling technique is tested using several special cases of common deformation textures for commercial beta-titanium alloys. It is demonstrated that the differences in an initial material texture affect the recrystallization kinetics even when nucleation mechanisms and grain-boundary properties are assumed to be the same. By taking the properties of special boundaries into account, the classical JMAK (Johnson-Mehl, Avrami, and Kolmogorov) kinetics is reproduced better during the simulation, and the grain-size distributions within the recrystallized material are broadened.

1. Introduction

Many metallic structural materials are produced commercially via the thermomechanical processing of large ingots with coarse and often nonuniform starting grain size. The conversion of such ingots to obtain a fine recrystallized microstructure usually relies on the dynamic and static recrystallization, sometimes followed by the grain growth. Because these processes control the microstructure evolution, they are critical to the optimization of a subsequent fabrication or service properties. In particular, the static recrystallization often controls the average grain size and texture in deformed and heat-treated materials. Hence, the phenomenology and mechanisms of recrystallization have been studied extensively over the past several decades. This research and the latest developments in this subject are summarized in [1—3].

Recently, a substantial progress in the understanding of recrystallization phenomena has been achieved by using various analytical and numerical modeling approaches [4—11]. As a result, a qualitative, and sometimes quantitative, description of the microstructure and texture evolution during recrystallization has been developed [3, 12]. For example, it has become increasingly recognized that the microstructure and texture evolution during recrystallization are closely related [13, 14] and thus must be taken into account in the development of advanced modeling routines [15, 16].

In the recent work, such as [13], the quantitative approaches to describe an initial texture and to model the simultaneous evolution of a microstructure and a texture have been developed. Nevertheless, there appears to be no complete quantitative model which incorporates the complex microstructural features that control the recrystallization kinetics and the texture evolution in the case where a noticeably textured initial state is formed due to an inhomogeneous deformation. In such instances, the resulting heterogeneity in the stored-energy distribution leads to the heterogeneous nucleation of recrystallized grains. The heterogeneous nucleation and possibly the initial texture may both initiate the anisotropic growth of recrystallized grains. Hence, modeling procedures in these situations may be very complicated.

Motivated by recent efforts, the objective of the present work is to develop and validate a computer-modeling technique for the analysis of the microstructure and texture evolution during annealing. The proposed model, based on a 3D Monte-Carlo (Potts) approach, incorporates a complete description of a microstructure and a texture and takes into account both the recrystallization driven by the stored energy and the grain growth driven by the thermally activated grain-boundary migration. The usefulness of the analysis is established with reference to experimental observations for two commercial beta-titanium alloys.

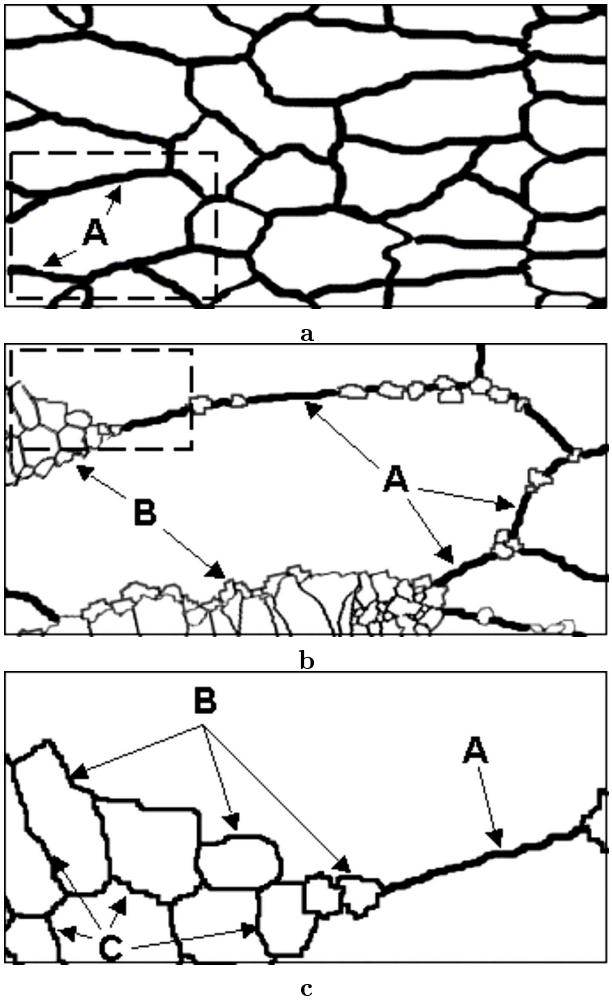

Fig. 1. Schematic illustration of the microstructure: (a) Prior to recrystallization, (b) selected area of (a) after recrystallization starts, and (c) selected area of (b) at a higher magnification

2. Description of Recrystallization Phenomena

In the present work, the recrystallization was treated in the typical manner as a process of nucleation and growth of new (recrystallized) grains. The migration of the grain boundaries within unrecrystallized volumes is also taken into account. These phenomena are depicted schematically in Fig. 1 and briefly described below.

2.1. Nucleation

Fig. 1,a shows the microstructure of a deformed material prior to the recrystallization. It is commonly observed that the recrystallization nuclei originate at inhomogeneities in the deformed microstructure, such as grain boundaries, shear bands, etc. The nucleation of new grains in the vicinity of prior grain boundaries, whose orientations are not related to orientations of one of the parent grains, has also been observed and is more common at larger strains [3, 17—19]. Hence, for the present study, the nucleation sites were chosen to be primarily associated with the grain boundaries of the deformed microstructure (Fig. 1,b) and secondarily with specific areas within the grains. The nucleation rate was specified using the following phenomenological relation:

$$\dot{N} = Z\left(H_{\Omega}(t) - H_{\min}(t)\right) V_n\left(t\right) \exp\left(\frac{-Q_A}{k_{\mathrm{B}}T}\right), \qquad (1)$$

in which H_{Ω} is the average stored energy of deformation, $H_{\min}(t)$ is the minimum stored energy that causes the recrystallization nucleation within the deformed material, $V_n\left(t\right)$ is the fraction of grain-boundary surface area on which nucleation is still possible at time t, Z is a constant, Q_A is the activation energy for nucleation, k_{B} is Boltzmann's constant, and is the absolute temperature.

Although it is generally accepted that the oriented nucleation occurs in most recrystallization cases, many details of how nuclei of particular orientations develop remain unclear. Hence, one can use experimentally derived orientation relationships between the texture of a deformed matrix and recrystallization nuclei in modeling instead of simulating individual nucleation events. Specific orientations of the recrystallization nuclei relative to the deformed matrix have been found in many experiments (Table 1) [2, 3, 19—23].

The specifics of boundary motion and stored work are summarized in the subsections that follow.

2.2. Grain-boundary migration

Fig. 1 presents three different types of grain boundaries considered in the modeling of recrystallization. Boundaries between the grains in the deformed material prior to recrystallization are denoted as type-A boundaries (Fig. 1,a); grain boundaries between the deformed matrix and recrystallized grains as type B (Fig. 1,b); and grain boundaries between recrystallized grains as type C (Fig. 1,c). Type-B boundaries form the recrystallization front.

The kinetics of the migration of grain boundaries of type C is controlled by the grain-boundary energy E and mobility M as well as by the local grain-boundary curvature R [15, 24]. The curvature-driven

grain-boundary velocity can be estimated from the following expression:

$$v \sim EMR^{-1}. \tag{2}$$

The average rate of migration of the boundary between grains G_i and G_j is

$$v_{G_iG_j} \sim E_{G_iG_j} M_{G_iG_j} \left(R_{G_i}^{-1} - R_{G_j}^{-1}\right) \quad , \tag{3}$$

in which R_{G_i} is the average grain-boundary curvature.

For type-B grain boundaries, the velocity of the recrystallization front moving into the unrecrystallized matrix can be described by [25]

$$v \sim M\left(-ER^{-1} + \Delta H\right), \tag{4}$$

where ΔH denotes the driving force for recrystallization in terms of the excess stored energy of deformation within the unrecrystallized grains in comparison with the recrystallized ones.

2.3. Grain-boundary energy and mobility

The existing experimental data on the dependence of the grain-boundary energy and mobility on the local lattice misorientation ε are sparse [26—29]. Even with the results collected in [29], it is not possible to fully describe the grain-boundary energy and mobility as functions of the exact grain-boundary misorientation. Nevertheless, from a qualitative perspective, all of the measurements are similar to those shown in Fig. 2 for the boundary energy and mobility as a function of the scalar misorientation.

It is often difficult to separate the specific contributions of energy and mobility to the overall grain-boundary kinetics [30, 31]. Hence, for modeling purposes, normalized, instead of actual, values of the energy $W\left(g_{G_i}, g_{G_j}\right) \equiv W(\varepsilon)$ and mobility $U\left(g_{G_i}, g_{G_j}\right) \equiv U(\varepsilon)$ of the grain boundary as a function of misorientation were used, viz.,

$$E = E_{\max} W(\varepsilon)$$

$$M = M_{\max} U(\varepsilon), \tag{5}$$

where $E_{\max}$ and $M_{\max}$ are the maximum possible grain-boundary energy and mobility, respectively. The values of $W(\varepsilon)$ and $U(\varepsilon)$ ($W(\varepsilon)$, $U(\varepsilon) \in [0..1]$) are used in determining the elementary orientation-flip probability in the present work.

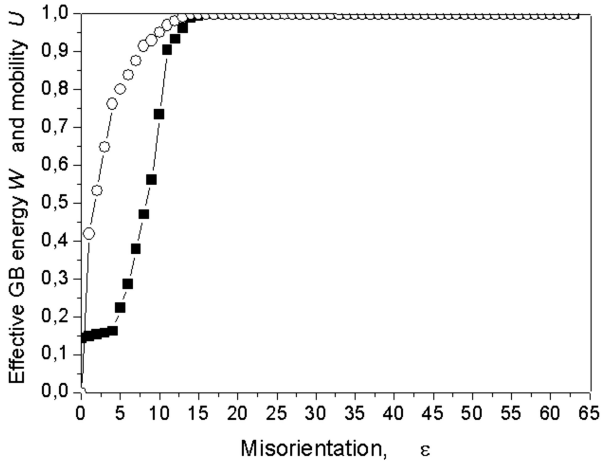

Fig. 2. Effective grain-boundary energy (○) and mobility (■) as a function of grain-boundary misorientation

2.4. Distribution of the stored energy in a deformed material

As described in Eq. (4), the grain-boundary motion is strongly dependent on the stored work which is nonuniformly distributed from grain to grain. The Taylor factor is the first-order approximation for the stored energy in a given grain.

During deformation, the grains of a polycrystalline metal change shape in a manner that corresponds approximately to the macroscopic shape change. This results in an increase in the grain-boundary area. The new grain-boundary area is continuously created during deformation by the incorporation of some of the dislocations generated during deformation. Hence, a certain part of the stored energy of the deformed material is associated with the grain boundaries. A high level of stored energy *within* given grains in the vicinity of grain boundaries and triple junctions (Fig. 3) has been clearly shown by electron back-scattered diffraction analysis (EBSD) [32]. The most stored energy is associated with dislocations which, however, are distributed nonuniformly within grains.

The dislocation density and therefore the stored energy can exhibit intragrain maxima and minima. The local dislocation-density (and, hence, stored-energy) maxima are often associated with intersecting slip bands [3]. It can thus be concluded that, in a plastically deformed material, the local stored energy associated with the volume element S_j often has its minimum at the center of a grain and its maximum close to the grain boundary. In the previous work [18], the MC simulations

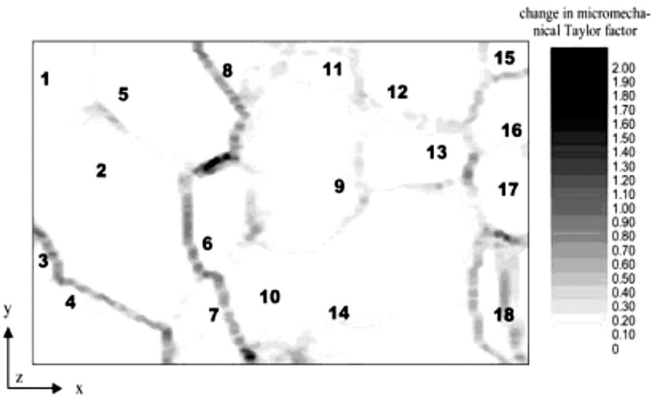

Fig. 3. Distribution of the largest component of the gradient of the "micromechanical Taylor factor", i.e., local stored-energy distribution reconstructed from EBSD data [32]. Strong effects appear in the vicinity of grain boundaries and triple junctions

were conducted for the recrystallization of a material with a non-uniform stored-energy distribution in the as-deformed microstructure. However, it is often not possible to quantify the stored-energy distribution from the FEM modeling, as was done in [18], or from measurements such as those based on the image quality of EBSD patterns. Hence, in the present work, a new analytical approach is used to describe the discrete distribution of stored energy within the deformed grains for the purpose of the 3D MC simulation of recrystallization within large modeling volumes. Specifically, consider a deformed bicrystal containing a single grain boundary. For the grains in such a bicrystal, the stored energy in unit volume S_j is given by the following relation:

$$\Delta H_{S_j} = Cf(\varepsilon, L) H_{\max}; \quad \sum_{i=1}^{k} \Delta H_{Sj} = M_T. \tag{6}$$

Here, the quantity f is a factor which depends on the misorientation and the distance from the grain boundary. It determines the level of ΔH at the grain boundary and the value of the stored-energy gradient close to the grain boundary. Ldenotes the distance to the grain boundary in the MC modeling units (MU), or the spacing between the MC lattice points; i.e., a model unit is equal to the length of the edge of the volume element S_j. $H_{\max}$ is the maximum possible value of the stored energy of deformation. M_T is a measure of stored energy; its value can be derived experimentally by integration of the local stored-energy distribution over the grain volume as determined from EBSD data [32] or neutron diffraction or by utilizing the correlations between the Taylor factor and the stored energy [33]).

To generalize Eq. (6) to the case of a real grain having a number of grain boundaries, the stored energy per unit volume comprises the superposition of the contributions from all boundaries, i.e.,

$$\Delta H_{S_j} = C_1 \left(\frac{1}{n} \sum_{i=1}^{n} f(\varepsilon_i, L_i) + P_{cr}(S_j) \right) H_{\max};$$

$$\sum_{i=1}^{k} \Delta H_{Sj} = M_T. \tag{7}$$

Here, n denotes the number of grain boundaries which form the given grain, and L_i are the nearest distances to the grain-boundary i in MUs. In other words, the first term in Eq. (7), depends on the average distance between the volume element and the nearby grain boundaries and on the misorientation, while the second term reflects the part of the dislocation-density distribution independent of the distance to the grain boundaries. The desired relation between the two parts of Eq. (7) can be achieved by varying $f(\varepsilon_i, L)$ and $P_{\rm cr}(S_j)$: (Fig. 4). In the simplest case, Eq. (7) can be readily modified to treat a *uniform* distribution of stored energy by omitting $P_{\rm cr}(S_j)$ and taking $f(\varepsilon_i, L) = f(\varepsilon_i)$. In the more general case, Eq. (7) with various sets of parameters can provide insight into how different stored-energy distributions affect recrystallization.

The movement and re-arrangement of dislocations due to the recovery-type processes (e.g., resulting from the climb and cross-slip of dislocations) can result in a significant reduction in the stored energy before the initiation of recrystallization. The recovery and nucleation of recrystallized grains are thermally activated processes; hence, temperature has a complex effect on the nucleation and the overall recrystallization kinetics. The nucleation rate increases rapidly with increasing temperature, as indicated by the exponential function in Eq. (1). On the other hand, the nucleation rate may decrease with increasing temperature due to the recovery processes that reduce the stored energy. Because the present work focuses on the texture and microstructure changes, rather than on the specific relationship between the simulation and real time scales, such recovery effects were not incorporated into the present modeling framework.

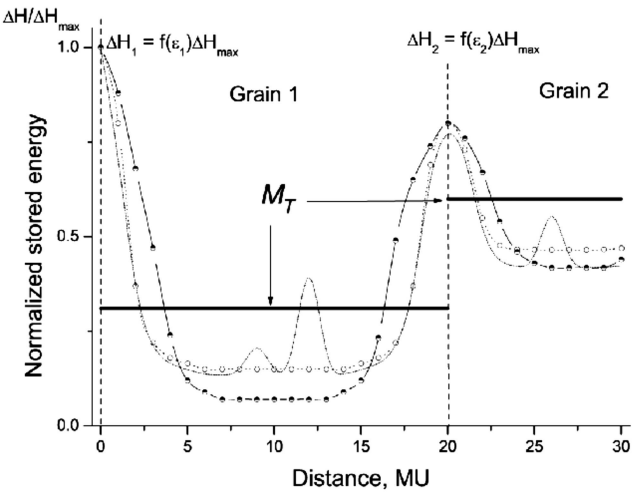

Fig. 4. Possible inhomogeneous stored-energy distributions across grains in the deformed microstructure

2.5. Recrystallization kinetics

From a phenomenological standpoint, the recrystallized fraction as a function of the annealing time usually exhibits a sigmoidal behavior. This can be expressed mathematically by the well-known JMAK relation [3, 14]

$$F = 1 - \exp\left(-Bt^k\right), \tag{8}$$

where F is the fraction recrystallized, B and k are constants, and t is time.

It should be noted that the grain growth within a recrystallized volume does not affect the recrystallized-fraction kinetics, but has a significant effect on the final material texture and microstructure.

3. Monte-Carlo Model for Recrystallization and Grain Growth

3.1. Selection of modeling approach

In the past, both the MC [4, 9, 25, 35] and the cellular-automaton (CA) [6,8,20] techniques have been used for the numerical simulation of recrystallization. Each technique has important restrictions, however. For instance, typical CA approaches are unable to account for the local grain-boundary curvature as a driving force for the grain-boundary migration [36]. On the other hand, the MC technique encounters problems in modeling the linear relationship between the stored-energy gradient and the migration rate of the

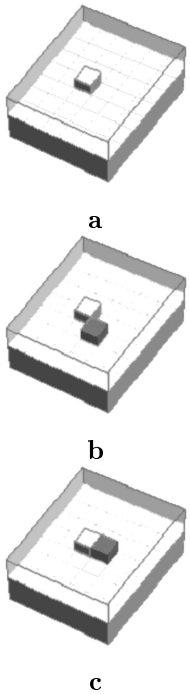

Fig. 5. Schematic illustration of the "model-lattice" effect: (a) State prior to the MC orientation flip and (b, c) different post-flip states that cannot be distinguished by standard MC approaches

recrystallization front due to the "model-lattice" effect. Because of this, the recrystallization and grain growth have often been treated separately using different techniques. Recently, there has been some initial success in formulating 2D hybrid-modeling approaches for modeling the grain-growth processes running in parallel with recrystallization [36].

Fig. 5 illustrates the nature of a discrete modeling volume, or "model-lattice" effect, that distorts the shape of the recrystallization front and the associated recrystallization kinetics during MC simulations. Specifically, consider the recrystallization-front shape prior to an MC trial (Fig. 5,a). Figs. 5,b and 5,c illustrate how two different lattice points, or the so-called MUs, can be selected within the unrecrystallized volume for the MC trial procedure. There is no difference between cases (b) and (c) in standard MC procedures; both MUs have the equal numbers of neighboring MUs that belong to the recrystallized and unrecrystallized volumes. It is also obvious that there is an equal change in the local stored energy for configurations (a) $\rightarrow$ (b) and (a) $\rightarrow$ (c) in the case where there is no significant gradient of stored energy along the horizontal plane in Fig. 5. However, the MUs selected for the flip trial in cases (b) and (c) have different 'coordination' relations with

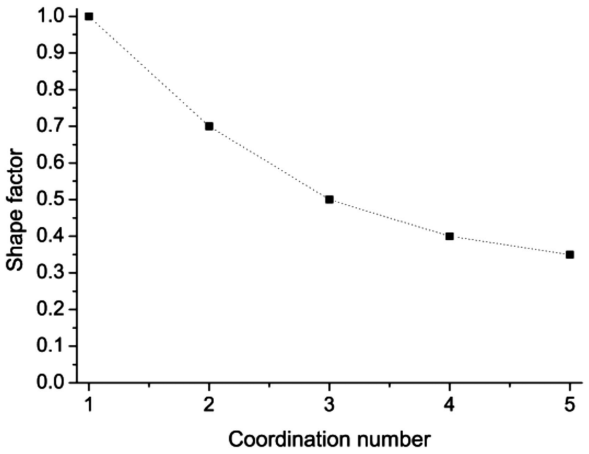

Fig. 6. "Shape factor" as a function of the MU coordination number. Values were obtained from MC simulations to form a smooth recrystallization front

respect to the upper MU in configuration (a). Hence, there must be a difference in the probabilities of MU reorientations in cases (b) and (c) in order to predict the recrystallization-front shape and the overall recrystallization kinetics. Ignoring this difference in standard MC approaches may result in noticeable distortions of the recrystallization front; e.g., the formation of bubbles, occlusions (as reported in [4]), "whiskers", etc. In contrast, the CA approach does not contain probabilistic trials and, hence, is free from this particular problem. As a result, MC simulations are usually not often used to simulate recrystallization.

One of the few attempts to use a "pure" MC approach to model the recrystallization was done in [14] for heavily cold-rolled aluminum. By using oblate grains with an aspect ratio of 64:8:1 in the initial microstructure, the model-lattice effect was avoided. Important details, such as the anisotropy of grain-boundary mobility and inhomogeneities in the stored-energy distribution within grains, were not taken into account, however. The simulation of the microstructure evolution in such an approach was not realistic because the newly formed nuclei had a diameter comparable to the thickness of the deformed grain. Hence, the model described in [14] was essentially suitable for the nucleation stage, but could only provide a qualitative information regarding the texture evolution.

An MC simulation technique was also employed to model the recrystallization and grain growth using a 2D modeling volume (with a triangular lattice array) in [25]. It was shown that the recrystallization front becomes unrealistically rough for high stored energies. Another

Fig. 7. MC-predicted growth of an isolated recrystallization nucleus within the unrecrystallized matrix after 30 MCS: a — without using a "shape factor" and b — using a "shape factor"

problem was the quality of the texture simulation for small modeling volumes. In other words, the number of grains in the deformed (initial) microstructure must be large enough to make the texture statistically representative; this can be difficult to do for small modeling volumes.

In the present work, the recrystallization features summarized in Section 2 are incorporated into an MC code. To overcome the model-domain lattice effect, a special local shape factor, $0 \leq F(\Omega_{S_i}) \leq 1$, was introduced into the MC procedure for determining the flip probability (Fig. 6). This factor provided a correction for the flip probabilities based on the distribution of differently oriented neighboring MUs and thus their coordination numbers. The dependence of the shape factor on the coordination number of the MU considered gives an advantage to arrangements such as 'c' in Fig. 5 as compared to arrangement 'b'. A validation trial (described below in Section 3.4) established that this new approach gives rise to a physically meaningful description of the migration of the recrystallization front and helps to overcome the formation of a rough recrystallization front (Fig. 7). Another distinguishing feature of the present simulations is the use of a substantially larger modeling volume consisting of 15,625,000 MUs, than that typically employed in prior investigations. By this means, the ODF and texture of the starting (deformed) condition are reproduced precisely in the 3D model domain.

3.2. Initial texture and grain structure for MC simulations

The MC model domain was formed by a 3D cubic array of MUs, each of which represented a point in the cubic lattice. The microstructure and texture evolution within the model domain (MD) was simulated as in the previous work utilizing the MC approach to describe the interaction of the grain growth and texture evolution

[15, 16]. In all calculations, the length of the side of the MD was set equal to 250 MUs; hence, the model domain was large enough to obtain an adequate statistical representation of the microstructure and texture.

In the most general 3D case, eight parameters are needed to unambiguously define a grain boundary; namely, three terms for the orientation relationship, two parameters for the spatial orientation of the grain boundary itself, and the three components of the translation vector that characterize the displacement of grains with respect to each other. To define the grain orientation with respect to the specimen (or model-domain) orientation, three Euler angles (φ_1, Φ, and φ_2 in the Bunge notation [37, 38]) were used. Specific values of the stored energy ΔH and the crystallographic orientation $g = \{\varphi_1, \Phi, \varphi_2\}$ ($0 \leq \varphi_1 < 360$, $0 \leq \Phi < 90$, $0 \leq \varphi_2 < 90$) were associated with each MU. The orientation space was divided into segments of $2 \times 2 \times 2$ degrees. The grain-boundary position was associated with the space between two sites having unlike orientations. Each grain was characterized by a volume equal to the number of MUs that comprised it.

A special procedure was developed to create the initial textural state in the model domain and thus to replicate the specified ODF as closely as possible. This procedure was based on the following probabilistic function:

$$P(\Omega_j) = \frac{1}{V_{\mathrm{MD}}} \frac{1}{N_g(\Omega_j)} \sum_{\mathrm{MD}} V(G_i,) \chi(g(G_i)),$$

$$\chi(g(G_i)) = \begin{cases} 1, & g(G_i) \in \Omega_j, \\ 0, & g(G_i) \notin \Omega_j, \end{cases} \qquad (9)$$

in which $g(G_i)$ is the orientation of the i-th MU, $V(G_i)$ is the number of MUs oriented as $g(G_i)$, N_g is the total number of orientations g within the volume Ω_j, and V_{MD} is the volume of the overall model domain. From the tests on model textures, it was determined that this procedure did not work well when the number of grains in the initial microstructure was less than 50, but it gave very good results when it was equal to 100 and more.

A stochastic procedure was developed to create the initial microstructure in the model domain and to replicate the experimentally observed microstructures with specific deformed-grain aspect ratios (for example, Fig. 8,*b*). For this purpose, the number of grains within the model domain was determined first from the average grain size. Then, we selected randomly the corresponding number of MU locations, at which the grains were to be created in the model volume. The remaining MUs were then assigned to these initial grains in a probabilistic manner; i.e., a randomly selected MU site, if not yet the part of a grain but adjacent to a specific grain, was assigned to this grain with a probability proportional to the prescribed aspect ratio. Such an approach enabled 99% of the model domain to be filled with grains. The remaining 1% of the MUs was then randomly assigned to adjacent grains. Then the stored energies were determined according to Eq. (7) for each MU.

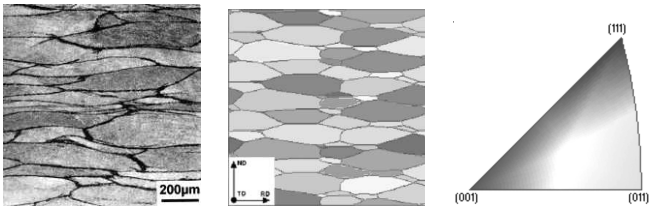

a **b** **c**

Fig. 8. *a* — optical microstructure of hot rolled Ti-6Al-2Sn-4Zr-6Mo [30], *b* — the corresponding inverse pole map for the 001 direction of the sheet used as a starting MC model microstructure, and *c* — the color key for the inverse pole-figure map

3.3. Grain-boundary misorientation in the MC simulations

The single parameter related to the lattice misorientation between neighboring grains was used to define the relative grain-boundary energy and mobility [see Eq. (5)]. The present modeling routine used the (approximate) scalar misorientation ε between grains having orientations $g_1$and g_2 [35], i.e.,

$$\varepsilon = \arccos\left(\frac{m_{11} + m_{22} + m_{33} - 1}{2}\right). \qquad (10)$$

Here, the elements m_{ij} form the matrix

$$\mathbf{M} = \mathbf{M}_{g_1} \times \mathbf{M}_{g_2}^{-1} = \begin{pmatrix} m_{11} & m_{12} & m_{13} \\ m_{21} & m_{22} & m_{23} \\ m_{31} & m_{32} & m_{33} \end{pmatrix}, \qquad (11)$$

and the rotation matrices $\mathbf{M}_{g_1}$, $\mathbf{M}_{g_2}$correspond to the orientations g_1 and g_2 [39,40]. If the lattice symmetry is higher than the triclinic one, we need to take into account the presence of equivalent rotations. For example, for bcc crystal structures, it is the smallest ε value from all possible pairs $\varepsilon\left((\mathbf{M}_{g_1})_p ; (\mathbf{M}_{g_2})_q\right)$, where $p, q \in [1...24]$ [39].

Unfortunately, the evaluation of a scalar misorientation would require much time if done for each MC trial, even using the effective calculation schemes such as that based on quaternions [41]. Therefore, the

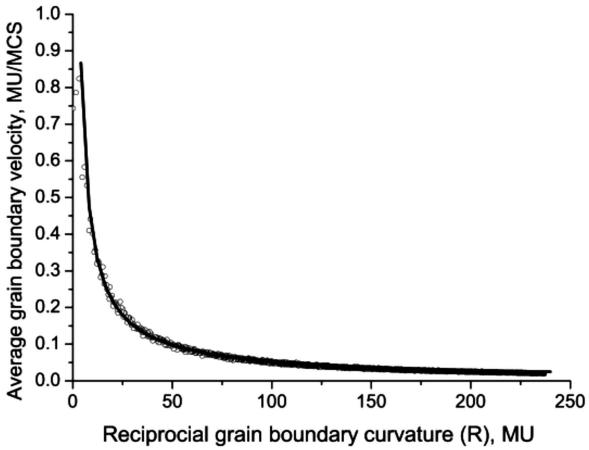

Fig. 9. Grain-boundary velocity as a function of the grain-boundary curvature in the absence of a stored-energy gradient: Solid line — Eqs. (*2*) and (*3*), circles — the MC simulation prediction

database of ε as a discrete function of g_1 and g_2 was calculated and loaded into the computer memory prior to the modeling. Thus, only the single search operation was performed for each MC trial.

3.4. Grain-boundary migration in the MC model

To simulate the boundary motion kinetics with the MC technique, an MU site was selected at random. Each unit was characterized by its set of Euler angles and ΔH value. If $\Delta H > 0$, the MU was assumed to belong to the unrecrystallized volume. A possible new MU orientation was then randomly selected from the orientations of adjacent grains (i.e. the adjacent MUs with orientations that differ from the orientation of the current MU). If the MU belonged to the recrystallization front and was already denoted as recrystallized, the new-orientation selection was restricted to the orientations of adjacent recrystallized grains. This was followed by a re-orientation attempt according to a typical MC trial procedure [15—16]. The local grain-boundary velocity is thus fully determined by the local conditions. Hence, the energy minimization for the entire model domain is equivalent to the energy minimization in the local area Ω_{Sj} close to the MU:

$$E_L = \frac{1}{2}\sum_{j=1}^{\Omega_n} W\left(\varepsilon_{S_i S_j}\right)\left(1-\delta_{S_i S_j}\right) + H_i, \qquad (12)$$

in which Ω_n denotes the number of MUs in the local area around the S_i model unit, and H_i is the stored energy associated with the model unit S_i.

The probability of a re-orientation of the S_i model unit from the state g_k to the state g_l is

$$P = \begin{cases} U(\varepsilon)W(\varepsilon)\exp\left(\frac{-\Delta E_L}{k_b T_l}\right), & \Delta E_L > 0, \\ U(\varepsilon)W(\varepsilon), & \Delta E_L \le 0; \end{cases}$$

$$\Delta E_L = E_L(g_l) - E_L(g_k); \varepsilon = \varepsilon(g_k, g_l). \qquad (13)$$

When an MU belongs to the recrystallization front and not yet denoted as recrystallized, we get

$$P = U(\varepsilon)\frac{\Delta H\left(S_i\right)}{\Delta H_{\max}} F\left(\Omega_{S_i}\right) \quad \exp\left(\frac{-\Delta E_L}{k_b T_l}\right), \qquad (14)$$

in which $F\left(\Omega_{S_i}\right)$ is the local shape factor for the MUs that belong to the recrystallization front.

The grain-boundary energy in most cases is 2 to 3 orders of magnitude *less* than the average stored energy ΔH [29] and thus is neglected in Eq. (14). As mentioned above, the factor $F\left(\Omega_{S_i}\right)$ represents the effect of the difference in coordination numbers of neighboring MUs on the flip probability for the current MC trial. The quantity T_l in Eqs. (13) and (14) denotes the "model lattice temperature" which is frequently introduced into MC simulations to overcome the lattice-pinning effects.

As a preliminary test of the MC routine and the validity of Eqs. (12) and (13) , the migration of an isolated 3D boundary with controlled curvature was performed. The good correspondence with Eq. (3) was obtained (Fig. 9).

3.5. MC procedure validation trial: Growth of an isolated recrystallized grain from a nucleus embedded in the homogeneous environment

A simple initial simulation was run to validate the MC routine. The objectives were to confirm the absence of the model-domain "lattice effect" and to test the quality of the random-number generator used in the MC routines. In this example, the grain boundary between the recrystallized phase (nucleus) and the deformed material (matrix) was of the $\Sigma 7$ type. The stored energy was distributed homogeneously in the deformed material.

The simulation results in this case are presented in Fig. 10. The recrystallization front maintained its spherical shape throughout the simulation, and there was a minimal deviation of the location of the center of a recrystallized grain as it grew.

4. MC Model Results for the Recrystallization of Engineering Titanium Alloys

Several modeling examples were run to verify the usefulness of the proposed MC-modeling approach. The specifics of the evolution of a recrystallization texture is mainly determined by the material texture under the starting (deformed) state and the preferred orientations of nuclei. As described in Sections 2 and 3, the recrystallization kinetics depends primarily on the average stored energy level, the nucleation rate, and the average grain size in the deformed state. In the present investigation, the assumed initial textures are similar to those of engineering beta-titanium alloys which have a bcc crystal structure. In all cases, the oriented continuous nucleation of recrystallized grains was assumed [3]. Furthermore, it was assumed that grain boundaries were preferred sites for the nucleation of recrystallized grains and that recrystallization nuclei had a special boundary of $\Sigma 7$, $\Sigma 9$, or $\Sigma 19$ type with one of the adjacent grains. The initial microstructure was assumed to comprise grains with a volume of 8000 MU^3 and an aspect ratio of 5:5:1.

All MC simulation cases were conducted for a material with anisotropic grain-boundary properties, i.e., misorientation-dependent grain-boundary energy and mobility (Fig. 2). The nucleation rate for each MCS within the unrecrystallized material was set assuming a constant nucleation rate of 10^{-4} nuclei/ MU^3. The recrystallization nuclei were assumed to be equiaxed (i.e., have an aspect ratio of 1:1:1) with an average volume of 15 MU^3. The simplest form of the function $f(\varepsilon_i, L)$ in Eq. (7) was used; namely, it was proportional to the grain-boundary misorientation. $P_{cr}(S_i)$ was assumed to be zero, i.e. no intra-grain maxima were introduced.

4.1. Case 1

In case 1, the initial texture within the model domain was homogeneous and replicated the common texture of cold-drawn Timetal LCB (Ti-4.5Fe-6.8Mo-1.5Al) (Fig. 11,*a*). The initial distribution of the stored energy within each grain (i.e., the parameters in Eq. (7)) was assumed to be inhomogeneous with the maximum values (between 0.7 and 1.0 x $\Delta H_{\max}$) at the grain boundaries. The stored energy in each grain decreased from the grain boundary toward the center (Fig. 4), at which ΔH had values between 0.2 and 0.4 x $\Delta H_{\max}$ depending on the grain size. The recrystallized grains nucleated in such a way to produce a $\Sigma 7$ boundary with one of adjacent grains.

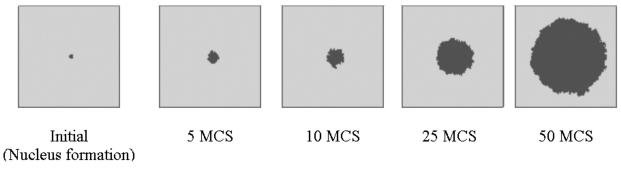

Fig. 10. 100 x 100 MU section from a 3D MC simulation of the growth of an isolated recrystallization nucleus

Fig. 12 summarizes the MC predictions of the microstructure evolution in case 1; different grain orientations are shown by different colors. From a qualitative standpoint, the inhomogeneous nature of the microstructure developed by the end of recrystallization, as indicated by the clustering of grains of similar colors/orientations, is evident.

The texture predictions in case 1 are summarized in Fig. 11. At the point at which the microstructure was 75%, the recrystallized (Fig. 11,*b*) transient texture maxima (circled) were formed; this finding is a result of the superposition of the initial axial texture components and the recrystallization components. As expected, these maxima vanished when recrystallization was complete and strong texture components, characterized by a rotation angle of $\pm 38.2°$ around the {111} direction, were formed (Fig. 11,*c*).

4.2. Cases 2 and 3

Cases 2 and 3 used the initial texture commonly found in a conventionally hot-rolled VT22 (Ti-5Al-5Mo-5V-1Cr-1Fe) sheet. Both cases assumed oriented-nucleation. In these instances, nuclei were able to form special grain boundaries of $\Sigma 7$, $\Sigma 9$, or $\Sigma 19$ type with one of the adjacent grains. However, different probabilities for each type of nucleus were used to determine the dependence of recrystallization texture on nucleation conditions, namely, $P(\Sigma 7) = 0.1$, $P(\Sigma 9) = 0.3$, $P(\Sigma 19) = 0.6$ in case 2 versus $P(\Sigma 7) = 0.6$, $P(\Sigma 9) = 0.2$, $P(\Sigma 19) = 0.2$ in case 3. The probabilities in case 2 approximate those previously found for the recrystallization of bcc materials (see the Table).

The microstructure-evolution predictions in cases 2 (Fig. 13) and 3 were similar. Some small evidence for the formation of spatially inhomogeneous textures was found, but such features were not as strong as in case 1.

Figure 14 summarizes the predicted ODFs for the simulated microstructures of cases 2 and 3 after 70 MCS.

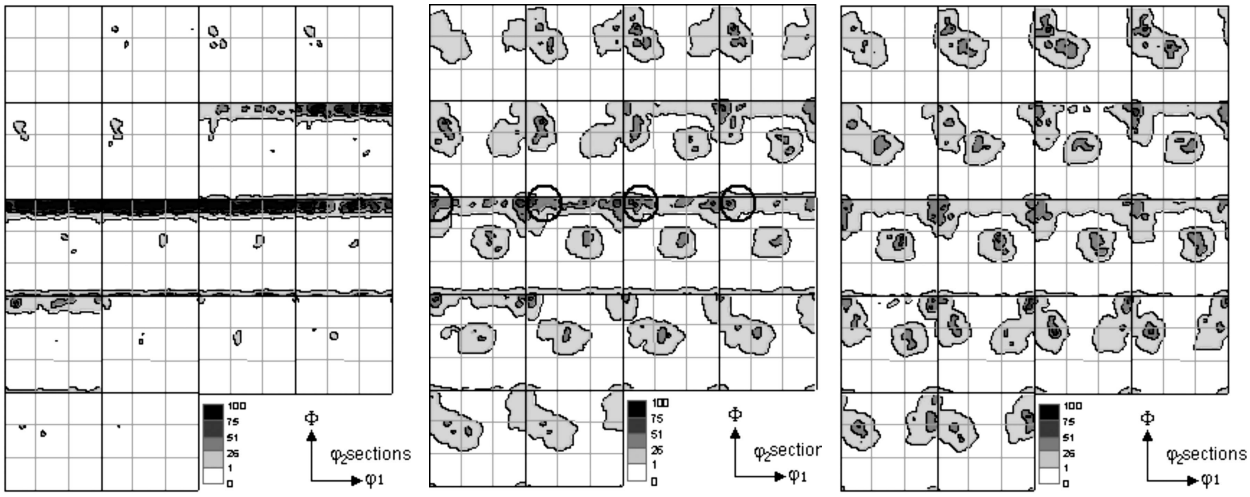

a **b** **c**

Fig. 11. MC predictions of the texture evolution in case 1: initial texture (*a*) and textures after 15 (*b*) and 100 MCS (*c*). The texture intensity is presented in terms of an x-random scale

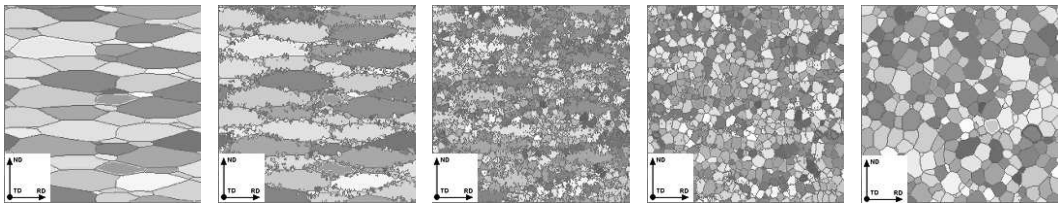

a **b** **c** **d** **e**

Fig. 12. MC-predicted microstructure evolution in case 1 (cross-section #125 of 250): initial structure (*a*) and microstructure after 5 (*b*), 50 (*c*), 100 (*d*), and 150 MCS (*e*)

The resulting textures had texture maxima at similar angular positions. However, the intensities of the texture maxima were found to depend on the nucleation probabilities for the two different cases.

Preferred orientations of recrystallized nuclei in terms of crystal lattice rotations relative to the deformed matrix orientation

Theoretical predictions [3]			Experimental measurements				
Σ	Angle (deg)	Axis	Angle (deg)	Axis	Metal	Lattice	Reference
Σ7	38.21	⟨111⟩	35—45	⟨111⟩	Al	f.c.c	[2,3,17—19]
			38	⟨111⟩	Cu	f.c.c	[3]
			36—42	⟨111⟩	Pb	f.c.c	[3]
Σ9	38.94	⟨110⟩	35	⟨110⟩	—	b.c.c.	[18]
Σ13a	22.62	⟨100⟩	23	⟨100⟩	Al	f.c.c.	[3]
			19	⟨100⟩	Cu	f.c.c	[3]
Σ13b	27.80	⟨111⟩	30	⟨111⟩	Cu	f.c.c	[3]
			30	⟨111⟩	Ag	f.c.c.	[3]
			20—30	⟨111⟩	Nb	f.c.c.	[3]
Σ17a	28.07	⟨110⟩	26—28	⟨100⟩	Pb	f.c.c	[3]
			30	⟨100⟩	Al	f.c.c.	[3]
Σ19a	26.53	⟨110⟩	25	⟨110⟩	—	b.c.c.	[2,18]
			27	⟨110⟩	Fe—Si	b.c.c	[3]
Σ19b	46.83	⟨111⟩	45	⟨111⟩	Al	f.c.c.	[19,46]
Σ21b	44.40	⟨112⟩	20—40	⟨112⟩	Al	f.c.c.	[2,3]
Σ27a	31.58	⟨110⟩	30	⟨110⟩	—	b.c.c.	[18]
—	—	—	24	⟨150⟩	Al	f.c.c.	[2,19]
—	—	—	oriented nucleation		Ti	b.c.c.	[42]

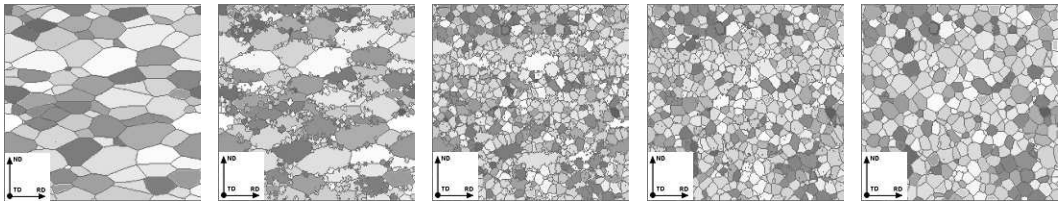

a b c d e

Fig. 13. MC-predicted microstructure evolution in case 2 (cross-section #125 of 250): initial microstructure (*a*) and microstructure after 5 (*b*), 15 (*c*), 50 (*d*), and 100 MCS (*e*)

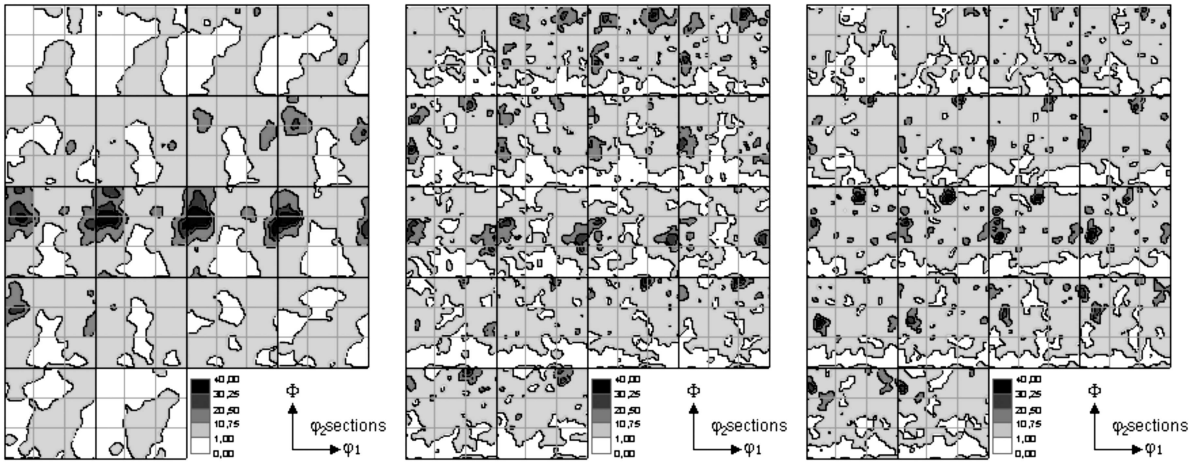

a b c

Fig. 14. MC predictions of the texture evolution in cases 2 and 3: initial texture (*a*) and textures after 70 MCS in case 2 (*b*) and case 3 (*c*). The texture intensity is presented in terms of an x-random scale

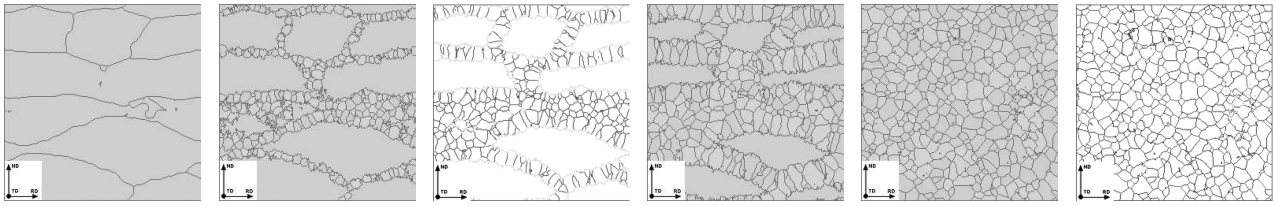

a b c d e f

Fig. 15. MC-predicted microstructure evolution in case 4 (cross-section #125 of 250): initial microstructure (*a*) and microstructure after 20 (*b*), 50 (*c*), 100 (*d*), and 250 MCS (*e, f*). Recrystallized grains which originate from the Σ7 nuclei are green (*b, d, e*). The grain boundaries are colored according to the scheme in Fig. 16 to indicate their effective mobility (*c, f*)

4.3. Case 4

This simulation was run to provide insight into the effect of the properties of special grain boundaries on the recrystallization kinetics. The initial grain structure and texture, as well as oriented-nucleation conditions, were assumed to be the same as in case 2. However, the initial grain size was assumed to be coarse (Fig. 15,*a*) in order to enable the easy visualization of the effective grain-boundary mobility during recrystallization (Fig. 15*c, f*). The effective grain-boundary mobility for special grain boundaries (Σ7, Σ9, and Σ19)) was assumed to be one-half that for arbitrary high-angle boundaries. Most of these special boundaries have a scalar misorientation between 25 to 37 degrees; hence, an effective mobility as shown in Fig. 16 was assumed in case 4. Nevertheless, it should be mentioned that the precise description of the properties of special boundaries is possible only by using

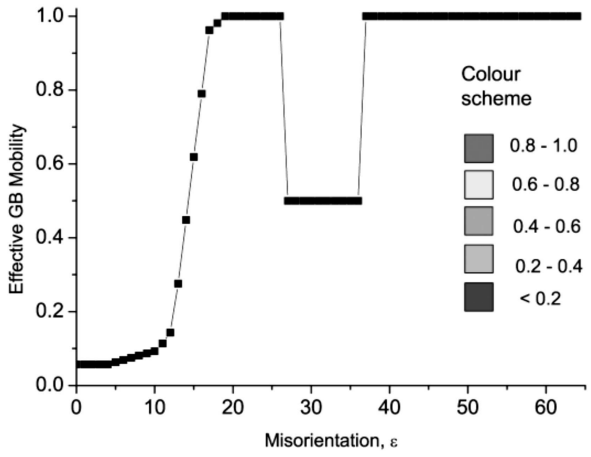

Fig. 16. Effective grain-boundary mobility as a function of the misorientation in case 4. The color scheme used in cross-sections of the simulated microstructures is also shown

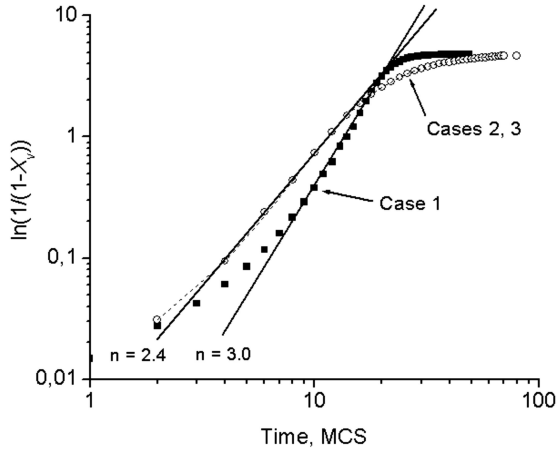

Fig. 17. Comparison of the MC predicted recrystallization kinetics in cases 1—3 (points) and a fit based on the JMAK relation [Eq. (8)] (solid lines)

the effective mobility as a function of the exact misorientation. However, this function has been estimated only for some points and rotations about high-symmetry lattice directions, but not for all misorientation space. Therefore, the proposed approach accounted for special boundaries in the average sense only.

Figure 15 summarizes the predictions of the microstructure evolution in the RD-ND plane of the sheet in case 4. Texture evolution in case 4 was predicted to be the same as in case 2.

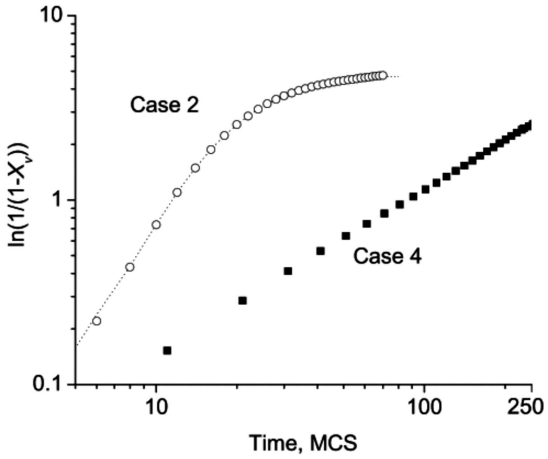

Fig. 18. Comparison of the MC-predicted recrystallization kinetics in cases 2 and 4

4.4. Recrystallization kinetics

Avrami plots (Figs. 17, 18) were made to quantify the overall recrystallization kinetics for the three different cases. The predicted kinetics in case 1 was noticeably different from those in cases 2 and 3 due to the stronger initial texture. Because the nucleation rate was assumed to be the same in all cases, the similar kinetics predicted by the MC model in cases 2 and 3 demonstrated that the initial texture is the main factor controlling the kinetics, even when the different probabilities of the oriented nucleation cause differences in the recrystallized material texture. The predicted recrystallization kinetics in cases 2 and 4 are compared in Fig. 18. The kinetics in case 4 is much slower than that in case 2, but provides a much better fit to the classical JMAK behavior.

The predicted Avrami exponents varied from 2.0 to 3.0. These predictions agree well with experimental data and modeling results in several previous investigations [3, 29, 43, 44], keeping in mind that the experimental slope usually reflects the JMAK kinetics in the vicinity of a fraction recrystallized of 0.65 [45]. The slowing of recrystallization in comparison with the ideal JMAK kinetics after the recrystallized volume fraction reached ~80—85% was probably a result of the discrete nature of the model domain as well as approximations concerning the mobility dependence on misorientation. Such an effect is typical in numerical simulations of recrystallization [43].

4.5 Recrystallized grain-size distributions

MC predictions of the grain-size distribution (GSD) within the recrystallized modeling volume in cases 1–4

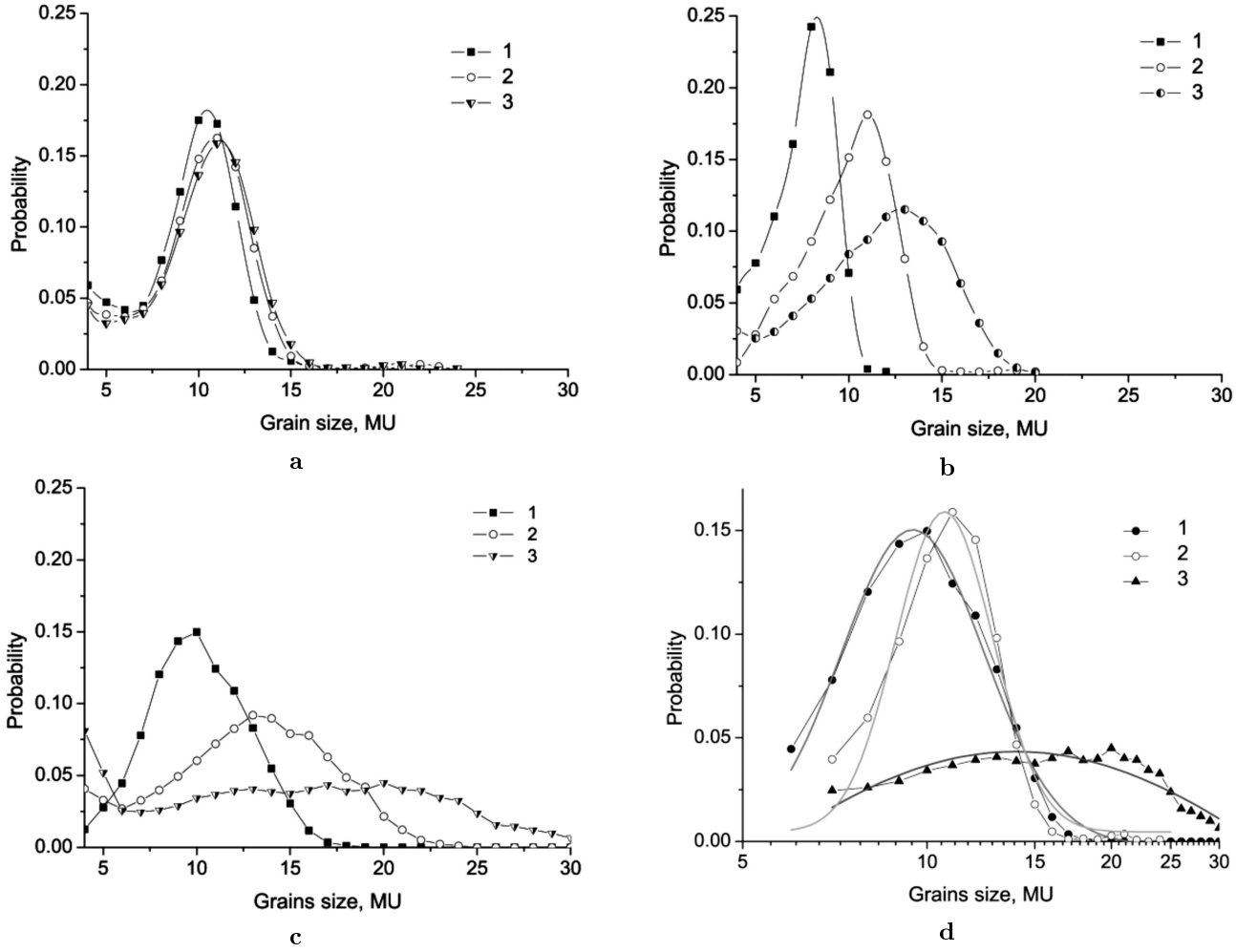

Fig. 19. MC-predicted grain-size distributions in case 1 (*a*), cases 2 and 3 (*b*), and case 4 (*c*) corresponding to recrystallized volume fractions of 20 (*1*), 50 (*2*), and 90% (*3*). MC-predicted grain-size distributions are compared in (*d*) to the classical log-normal distributions (smooth solid lines) [3, 47]: *1* — case 4, 20% recrystallized, *2* – case 1, 90% recrystallized, and *3* — case 4, 90% recrystallized

at 20, 50, and 90% fraction recrystallized are summarized in Fig. 19,(*a-c*). As for the recrystallization kinetics, the predicted GSDs in cases 2 and 3 were the same. In all cases, the width of the GSD increased with the fraction recrystallized; however, this trend was less pronounced in case 1 due to the large fraction of low-angle grain boundaries which were formed between recrystallized grains. On the other hand, a much bigger initial grain size relative to the size of recrystallization nuclei in conjunction with a large fraction of high-angle boundaries within the recrystallized volume led to the pronounced growth of recrystallized grains and eventually to a very broad GSD, as in case 4.

Some of the simulated GSDs are replotted and compared to the ideal log-normal distribution [47] in Fig. 19,*d*. This comparison reveals that the simulated GSD results are realistic with respect to the log-normal distribution usually found experimentally in recrystallized microstructures [3, 48].

5. Summary and Conclusions

The recrystallization of polycrystalline metallic materials was modeled using a 3D Monte-Carlo (Potts) approach, in which the initial microstructure, texture (ODF), spatial distribution of the stored energy of deformation, and nucleation mechanism are incorporated. Several simulations were performed to confirm the validity of the approach, namely the simulation of the growth of an isolated nucleus and the

recrystallization of real materials when only specially oriented nuclei are allowed to grow. It is shown that the model predictions are in good agreement with the theoretical JMAK kinetics and yield realistic grain-size distributions for the recrystallized microstructure. By taking the properties of special boundaries into account, even in an approximate manner, the better predictions of the classic JMAK recrystallization kinetics are obtained in the present approach.

The advanced 3D MC approach proposed in the present work provides a powerful tool to describe the effect of an inhomogeneous distribution of stored energy within the grains on recrystallization which is based on the average Taylor factor and phenomenological parameters introduced to emulate intragrain gradients. However, the lack of quantitative experimental data about such distributions poses an important challenge in the precise validation of the model, thus warranting a future research.

The present work was partially supported by the Air Force Office of Scientific Research (AFOSR) and the AFOSR European Office of Aerospace Research and Development (AFOSR/EOARD) within the framework of STCU Partner Project P-057.

1. *Recrystallization* of Metallic Materials/Ed. by F.Haessner. — Stuttgart: Riederer, 1978.
2. *Doherty R.D., Hughes D.A., Humphreys F.J.et al.* // Mater. Sci. Eng. A. — 1997. — **238** — P.219—274.
3. *Humphreys F.J., Hatherly M.* Recrystallization and Related Annealing Phenomena. — Oxford: Elsevier, 1995.— P.85—126, 173—220.
4. *Srolovitz D.J., Grest G., Anderson M.P., Rollett A.D.* // Acta met. — 1986. — **34**.— P.1833
5. *Erukhimovitch V., Baram J.* // Mater. Sci. Eng. A. — 1996. — **214** — P.78.
6. *Goetz R.L., Seetharaman V.* // Metall. and Mater. Trans. — 1998. — **29A**. — P. 2307—2321.
7. *Goetz R.L., Seetharaman V.* // Scr. mater. — 1998. — **38**. — P.405.
8. *Marx V., Reher F.R., Gottstein G.* // Acta mater. — 1999. — **47**. — P.1219.
9. *Radhakrishnan B., Sarma G.B., Zacharia T.* //Ibid. — 1998. — **46**.— P.4415—4433.
10. *Zurob H.S., Hutchinson C.R., Brechet Y., Purdy G.* // Ibid. — 2002. — **50**.— P.3075—3092.
11. *Stuwe H.P., Padilha A.F., Siciliano Jr.F.* // Mater. Sci. Eng. A. — 2002. — **333**. — P.361—367.
12. *Cahn R.W.* //Physical Metallurgy /Ed. by R.W.Cahn and P.Haasen.— Amsterdam: Elsevier, 1996.— Vol. **3**.— P.2400—2492.
13. *Caleyo F., Baudin T., Penelle R.* // Scr. mater. —2002. — **46**. — P.829.
14. *Rajmohan N., Szpunar J.A.* // Acta mater. — 2000. — **48**. — P.3327.
15. *Ivasishin O.M., Shevchenko S.V., Vasiliev N.L., Semiatin S.L.* //Ibid. — 2003. — **51**. — P.1019—1034.
16. *Ivasishin O.M., Shevchenko S.V., Vasiliev N.L., Semiatin S.L.* // Metalofiz. Noveishie Technol. — 2001. — **23**. — P.1569—1587.
17. *Bate P.S., Hutchinson W.B.* // Scr. mater. — 2005. — **52**. — P.199—203.
18. *Radhakrishnan B., Sarma G.B., Zacharia T.* // Acta mater. 1998. — **46**. — P.4415—4433.
19. *Hutchinson W.B.* //Acta met. — 1989. — **37**.— P.1047.
20. *Gottstein G., Sebald R., J. Mat.* // Proc. Technol.— 2001. — **117**. — P.282—287.
21. *Sebald R., Gottstein G* // Acta mater. — 2002. — **50**. — P.1587—1598.
22. *Ferry M. and Humphreys F.J.* //Ibid. — 1996. — **44**. — P.3089—3103.
23. *Engler O.* // Scr. mater. — 1997. — **37**. — P.1675—1683.
24. *Gordon P.* Energetics in Metallurgical Phenomena — New York: Gordon and Breach, 1962.— Vol. **1**.— P.207.
25. *Okuda K., Rollett A.D.* Microstructure Modeling and Prediction During Thermomechanical Processing/Eds. R. Srinivasan, S.L. Semiatin, A. Beaudoin, S. Fox, and Z. Jin. — 2001.— P.57—66.
26. *Winning M., Gottstein G., Shvindlerman L.S.* // Acta mater.— 2002. — **50**. — P.353—363.
27. *Wolf D.* // Acta metall. mater. — 1990. — **38**.— P.781.— P.791.
28. *Shewmon P.G.* Recrystalization, Grain Growth, Textures. — Metals Park, OH: ASM, 1966.— P.165.
29. *Gottstein G., Shvindlerman L.S.* Grain Boundary Mobility in Metals. — CRC Press, 1999.
30. *Weaire D., McMurry S.* Solid State Physics: Advances in Research and Applications /Eds. M. Ehrenreich and F. Spaepen. — San Diego, CA: Acad. Press, 1996.— Vol. **50**.— P.1.
31. *Gordon P., Vandermeer R.A.*//Ibid.— P.205.
32. *Raabe D., Sachtleber M., Zhao Z., Roters F., Zaefferer S.* // Acta mater. — 2001. — **49**. — P.3433—3441.
33. *Rajmohan N., Hayakawa Y., Szpunar J., Root J.* // Physica B. — 1998. — **241—243**. — P.1225—1227.
34. *Lutjering G., Williams J.C.* Titanium. — Berlin: Springer-Verlag, 2003.
35. *Song X., Rettenmayr M.* // Mater. Sci. Eng. A. — 2002. — **332**. — P.153—160.
36. *Rollett A.D., Raabe D.*// Computational Mater. Sci. —2001. — **21**. — P.69—78.
37. *Bunge H.J.*// Materials Science. — London: Butterworth, 1982.
38. *Bunge H.J.* Quantitative Texture Analysis /Eds. H.J. Bunge and C. Esling. — Oberursel: DGM-Informationsgesellschaft.— 1981.— P.1.

39. *Zhu G., Mao W., Yu Y.* // Scr. mater. — 2000. — **42**. — P.37—41.

40. *Glavicic M.G., Kobryn P.A., Bieler T.R., Semiatin S.L.* // Mater. Sci. Eng. A.— 2003. —**346**. — P.50—59.

41. *Sutton A.P., Balluffi R.W.* Interfaces in Crystalline Materials. — Oxford: Clarendon Press, 1995.

42. *Thibon I., Prima F., Texier G., Gloraint T., Ansel D.*// Proc. 10th World Conf. on Titanium/Eds. G. Lutjering and J. Albrecht.— Hamburg: DGM, 2003.— Vol. II.— P.1323.

43. *Uranga P., Fernandez A.I., Lopez B., Rodriguez-Ibabe J.M.* // Mater. Sci. Eng. A. — 2003. — **345**. — P.319—327.

44. *Rollett A.D.* // Progress in Mater. Sci.— 1997. — **42**. — P.79—99.

45. *Valencia Morales E., Vega L.J., Villar C.E.et al.* // Scr. mater. — 2005. — **52**.— P.217—219.

46. *Sabin T.J., Winther G., Jull Jensen D.* //Ibid. — 2003. — **51**. — P.3999—4011.

47. *Kurtz S.K., Carpay F.M.A.* // J. Appl. Phys. — 1980.— **51**.— P.5725.

48. *Saetre T., Hunderi O., Nes E.* // Acta met. — 1986. — **34**. — P.981.

Received 05.05.05

ТРИВИМІРНЕ МОДЕЛЮВАННЯ МЕТОДОМ МОНТЕ-КАРЛО (МОДЕЛЬ ПОТТСА) РЕКТРИСТАЛІЗАЦІЇ ТА РОСТУ КРИСТАЛІЧНОГО ЗЕРНА У ПОЛІКРИСТАЛІЧНИХ МАТЕРІАЛАХ

О.М. Івасишин, Н.Л. Васильєв, С.В. Шевченко, С.Л. Семятін

Р е з ю м е

Рекристалізацію полікристалічних металічних матеріалів промодельовано з допомогою тривимірної моделі Монте-Карло (модель Потса). У розробленому оригінальному підході до моделювання враховано вихідну мікроструктуру матеріалу, вихідний текстурний стан (у вигляді функцій розподілу кристалітів за орієнтаціями), просторовий розподіл накопиченої енергії пластичної деформації та механізм утворення зародків рекристалізації в об'ємі зразка. Передбачено формування мікроструктурних та текстурних неоднорідностей у рекристалізованому однофазному металічному матеріалі. З використанням розробленого підходу проведено моделювання процесів рекристалізації у комерційних титанових сплавах. Показано, що різниця у вихідному текстурному стані матеріалу суттєво впливає на кінетику рекристалізації, навіть за умови тотожності механізмів зародження рекристалізованої фази та властивостей міжзеренних меж. Встановлено, що при врахуванні особливостей поведінки спеціальних міжзеренних меж модельована кінетика рекристалізації найкраще відповідає класичному кінетичному рівнянню, а дисперсія розподілу зерен рекристалізованої фази за середніми розмірами збільшується.